Date: September 09, 2021

Influences of ALD Al$_2$O$_3$ on the surface band-bending of c-plane, Ga-face GaN and the implication to GaN-collector npn heterojunction bipolar transistors

Jiarui Gong[1], Jisoo Kim[2], TienKhee Ng[3], Kuangye Lu[4], Donghyeok Kim[2], Jie Zhou[2], Dong Liu[2], Jeehwan Kim[4], Boon S. Ooi[3], and Zhenqiang Ma[2,a]

[1]*Department of Physics, University of Wisconsin-Madison, Madison, Wisconsin, 53706, USA*

[2]*Department of Electrical and Computer Engineering, University of Wisconsin-Madison, Madison, Wisconsin, 53706, USA*

[3]*Department of Electrical and Computer Engineering, King Abdullah University of Science and Technology, Thuwal 23955-6900, Saudi Arabia*

[4]*Department of Mechanical Engineering, Department of Materials Science and Engineering, Massachusetts Institute of Technology, Cambridge, Massachusetts, 02139, USA*

[a] Author to whom correspondence should be addressed. Electronic mail: mazq@engr.wisc.edu

Abstract

Due to the lack of effective p-type doping in GaN and the adverse effects of surface band-bending of GaN on electron transport, developing practical GaN heterojunction bipolar transistors has been impossible. The recently demonstrated approach of grafting n-type GaN with p-type semiconductors, like Si and GaAs, by employing ultrathin (UO) Al_2O_3 at the interface of Si/GaN and GaAs/GaN, has shown the feasibility to overcome the poor p-type doping challenge of GaN by providing epitaxy-like interface quality. However, the surface band-bending of GaN that could be influenced by the UO Al_2O_3 has been unknown. In this work, the band-bending of c-plane, Ga-face GaN with UO Al_2O_3 deposition at the surface of GaN was studied using X-ray photoelectron spectroscopy (XPS). The study shows that the UO Al_2O_3 can help in suppressing the upward band-bending of the c-plane, Ga-face GaN with a monotonic reduction trend of the upward band-bending energy from 0.48 eV down to 0.12 eV as the number of UO Al_2O_3 deposition cycles is increased from 0 to 20 cycles. The study further shows that the band-bending can be mostly recovered after removing the Al_2O_3 layer, concurring that the change in the density of fixed charge at the GaN surface caused by UO Al_2O_3 is the main reason for the surface band-bending modulation. The potential implication of the surface band-bending results of AlGaAs/GaAs/GaN npn heterojunction bipolar transistor (HBT) was preliminarily studied via Silvaco® simulations.

Keywords: X-ray photoelectron spectroscopy, gallium nitride, ultrathin-oxide, band-bending, simulation, heterojunction bipolar transistor.

Introduction

For its high breakdown electrical field (4.9 MV/cm) [1] and high electron saturation velocity (1.4x10^7 cm/s) [2], gallium nitride (GaN) has been the semiconductor material enabling the highest-performance solid-state radiofrequency (RF) electronic device at present [3]. Although GaN-based high electron mobility transistors (HEMT) have been well-developed over the last two to three decades since its first demonstration [4], the ultimate electronic potential of GaN for both RF and power electronic applications may be eventually exploited from bipolar junction transistors (BJTs) [5]. With a vertical three-dimensional current flow from emitter to collector and the exponential dependence of the collector current density on the bias, BJTs based on GaN are theoretically expected to provide a much higher current density than that of the GaN-based HEMTs. However, limited by the well-known poor p-type doping in GaN, the most critical challenge, implementing practical GaN-based BJTs has been impossible to date [6]. In additional to this major challenge, the preliminary investigations of GaN-based BJTs revealed that the surface energy band-bending of GaN needs to be taken into crucial consideration for GaN-collector bipolar transistor applications [7, 8].

Considering the fundamental physics limit of realizing effective p-type doping in GaN, an alternative approach to tackle the p-type doping challenge in GaN-based BJTs development is to replace p-type nitride materials with other p-type semiconductor materials, such as silicon (Si), germanium (Ge), indium phosphide (InP), gallium arsenide (GaAs), etc. and employ these p-type materials as the base region of GaN-based bipolar transistors. Nevertheless, the lattice mismatch between these p-type materials and GaN prevented the epitaxial growth of GaN [9, 10] and wafer bonding/fusion approach [7, 8] from producing an abrupt junction/interface between GaN and the p-type semiconductors with a low interface density of states. The recently demonstrated semiconductor grafting approach [11], which, in terms of the working mechanisms, fundamentally distinguishes itself from the heteroepitaxy and the wafer bonding/fusion approaches, has solved the lattice-mismatch challenge. The insertion of an ultrathin oxide (UO) (e.g.,

Al$_2$O$_3$) layer between GaN and semiconductors with good p-type doping provides an abrupt junction with a very low interface density of states, manifested by the ideal p-n junction diodes characteristics. The p-n junctions formed by the grafting approach, featured with a p-n diode ideality factor (*n*) of ~ 1.10, ultra-low reverse-bias current density, record-high current on/off ratio values, avalanche breakdown characteristics, etc. rival those of the epitaxially grown, lattice-matched p-n junctions. Following the grafting approach [11], record-breaking III-nitride devices [12-14] and preliminary pnp AlGaAs/GaAs/Diamond HBT [15] have been reported.
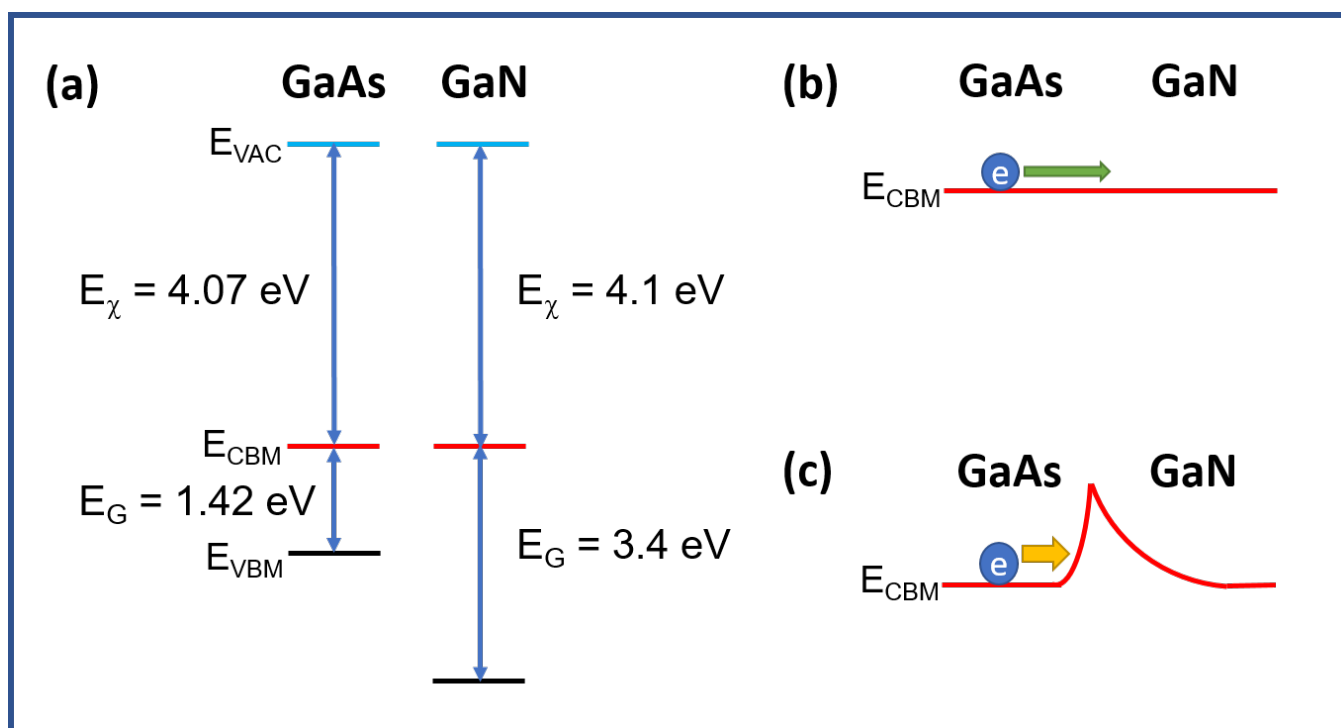

Fig. 1. Illustration of band alignment between GaAs and GaN and the influence of surface band-bending on electron transport from GaAs to GaN. (a) Band structures of GaAs and GaN (assuming no band-bending) before joining them together. Conduction band alignment between GaAs and GaN (b) without polarization induced band-bending and (c) with polarization induced band-bending in GaN. Due to the band-bending (c), electron transport from GaAs to GaN is blocked.

While the UO Al_2O_3 has been shown to play a critical role in the grafting method to achieve epitaxy-like lattice-mismatched heterojunctions between good p-type semiconductors and n-type GaN, achieving GaN-collector heterojunction bipolar transistors (HBTs) via grafting is not straightforward unless proper band alignment is realized between the constituent materials. For a npn GaN-collector HBT, like an AlGaAs/GaAs/GaN HBT, the conduction band alignment between the three materials needs to facilitate electron transport from emitter to collector. Since GaN exhibits surface energy band-bending due to polarizations and other associated effects., the band alignment of a grafted AlGaAs/GaAs/GaN may not favor the electron transport for HBT action. Fig. 1(a) shows the band diagrams of GaAs and GaN before they were grafted. Without considering the band-bending of GaN, GaN has an electron affinity of 4.1 eV [16] and a bandgap energy of 3.4 eV [17]. By grafting GaAs with GaN to form an epitaxial quality interface, the expected band alignment between the GaAs and GaN is illustrated in Fig. 1(b) without considering polarization. However, due to the polarization of GaN (c-plane, Ga-face) and the consequent upward band-bending, an energy barrier was formed at the conduction band between GaAs and GaN, as shown in Fig. 1(c). The energy barrier height is predominantly related to the GaN polarization strength, which can be affected by many factors. As a result, if forming/fabricating a npn AlGaAs/GaAs/GaN HBT via grafting without considering the band-bending of GaN, the energy barrier at the base-collector junction would block the electron current transport from the base region (p-GaAs) to the collector region (n-GaN), leading to poor or no transistor actions.

Previous studies have shown that the Al_2O_3/Ga-face GaN interface in metal-oxide-semiconductor (MOS) capacitors has a net positive charge [18-20] while a 0.4 eV upward band-bending was reported for the UO Al_2O_3-coated Ga-face GaN surface [21]. Although the mechanism of charge compensation at the Al_2O_3/Ga-face GaN interface is still under debate [22], these studies indicated the possibility to modulate the fixed charge density on the surface by UO Al_2O_3 and thus to reduce the surface band-bending of the c-plane, Ga-face GaN, potentially making GaN more suitable for HBT application. However, the results

of these previous studies are not applicable to the envisioned GaN-collector HBT applications that can be enabled by the grafting approach due to the different interface treatment conditions (e.g., oxide thickness, annealing temperature, etc.). Therefore, it is imperative to perform a thorough examination of the influence of UO Al_2O_3 and related thermal process, which is relevant to grafting for GaN-collector HBTs, on the band-bending of c-plane, Ga-face GaN.

In this work, we present the surface band-bending studies of c-plane, Ga-face GaN grown on a sapphire substrate with different UO Al_2O_3 thicknesses that is directly relevant to grafting, ranging from 0 to 20 cycles by atomic layer deposition (ALD) with/without post-deposition annealing (PDA). The PDA parameters were selected based on the optimized processing conditions for grafting [11]. X-ray photoelectron spectroscopy (XPS) was employed to measure the valence band maximum (VBM) energy for calculating band-bending and with which surface band-bending values were derived. To help understand the implication of the band-bending modification, preliminary simulations of an AlGaAs/GaAs/GaN npn HBT with the measured band-bending values from this study were performed using Silvaco®.

Experiment

The epitaxial n-GaN (~ 250 nm thick) employed in this study was epitaxially grown on a two-inch sapphire substrate with a doping concentration (Si dopants) of 1×10^{18} cm^{-3}, which was characterized by secondary-ion mass spectroscopy (SIMS). With this doping concentration, the Fermi level (E_F) was calculated to be 0.005 eV (($E_{CBM} - E_F)_{GaN}$ or $q\phi_{B,GaN}$) below the conduction band minimum (CBM). In this study, the epitaxial n-GaN wafer was used throughout the study under seven different surface treatment recipes. The cleaning of the n-GaN epi for all recipes of the study follows identical procedures: acetone, IPA, and DI water for 10 minutes, followed by 5 minutes of piranha etching (96% H_2SO_4 : 30% H_2O_2 : H_2O = 1:1:8), 10 minutes of diluted hydrochloric acid etching (0.1 normal HCl : H_2O = 1:1), and

5 minutes of diluted hydrofluoric acid etching (49% HF : H_2O = 1:1) to remove the surface oxide (all the ratios are based on volume). For recipe #1-start, the n-GaN epi, which was a bare sample case without UO Al_2O_3, was immediately loaded for XPS analysis after cleaning. For recipes #2 to #7, the epi sample was loaded into the ALD chamber after cleaning. For ALD depositions, the ALD stage was heated to 200 °C and 5 cycles of trimethylaluminum (TMA) precursor flow was run with the purpose of in-situ native oxide removal, followed by Al_2O_3 deposition using the TMA precursor and H_2O vapor under the same temperature of 200 °C. Each recipe has a different number of ALD deposition cycles. The expected ALD Al_2O_3 growth per cycle (GPC) is ~ 0.1 nm/cycle, although not strictly accurate for the initial cycles [23]. For recipes #2, #4, #6 and #7, XPS analyses were conducted directly after ALD deposition. For recipes #3 and #5, the sample was annealed in N_2 ambient at 350 °C for 5 minutes (post-deposition annealing (PDA)) before performing XPS analyses. After finishing the XPS analysis of recipe #7 (20 ALD deposition cycles), the Al_2O_3 of the epi sample was removed to make it a bare sample (recipe #1-end) again, and the bare n-GaN was analyzed using XPS. All ALD deposition and PDA conditions are identical to those used in the grafting of GaAs/GaN [11]. Table 1 summarized the detailed conditions of each recipe. Atomic force microscopy (AFM) analyses were conducted on the surface of the epi sample after each surface treatment using recipes #1, #2 and #3 (Fig. S1), revealing unchanged surface roughness. Combined with the XPS spectra of Al 2p (Fig. S1), it is confirmed that a smooth layer of Al_2O_3 was deposited on top of the GaN, consistent with the high-resolution transmission electron microscope (HRTEM) images of the grafted pn diodes [11]. Raman spectroscopy analyses were performed to assess the strain status of the n-GaN on sapphire epi sample under surface treatment recipe #1 and #7 (Fig. S2). It was found that the same amount of compressive strain exists for both recipes, matching the reported value of GaN epitaxial materials grown on sapphire substrates [24].

The XPS characterizations were performed using a Thermo Scientific K Alpha X-ray Photoelectron Spectrometer with Al K$_\alpha$ X-ray source (hv = 1486.6 eV). The following settings were applied to the

spectrometer: 10 eV pass energy, 100 μm spot size, 40s dwell time, and 0.02 eV step size. The spectrometer was calibrated using the Au $4f_{7/2}$ peak and the charge correction was conducted using the C $1s$ peak at 284.6 eV [25]. The Au $4f_{7/2}$ spectrum was used to calculate the instrumental uncertainty. By fixing the full width at half maximum (FWHM) Lorentzian lifetime width Γ within the range of 0.30 eV to 0.34 eV for the Au $4f_{7/2}$ spectrum, a total Gaussian resolution σ, which includes the uncertainty from Gaussian phonon and that from the spectrometer itself, of 0.19 eV to 0.21 eV was fitted [25-27].

Results and discussion

Fig. 2(a) shows the recorded XPS spectrum of the n-GaN valence band directly from the XPS spectrometer under surface treated using recipe #1-start. The spectrum is also representative of all XPS spectra acquired from the studied recipes (Fig. S3). Based on the XPS spectra obtained, the binding energy of VBM at the surface of GaN ($(E_F - E_{VBM})_{GaN}$ or $q\phi_{S,GaN}$) was determined using the method developed by Reddy Pramod et al. [25, 28], as shown in Fig. 2(b). The theoretical density of state (DOS) for 3D hexagonal crystal lattice with consideration of nearby atoms can be calculated using the Monte Carlo method in the first Brillouin zone using the energy dispersion relation

$$E = \epsilon - t\big(2\cos(k_x a) + 4\cos(\sqrt{3}k_y a/2)\cos(k_x a/2) + 2\cos(k_z c)\big), \qquad (1)$$

where ϵ is the reference energy, t is the bond energy, and a and c are the lattice constants of GaN. This theoretical DOS (the red curve in Fig. 2(b)) is a good approximation of the XPS spectrum around the VBM (the black curve in Fig. 2(b)) after Gaussian broadening [25]. The DOS curve was then convoluted with a Gaussian broadening equation whose standard deviation is the total Gaussian resolution σ of the spectrometer. By matching the convoluted DOS curve (the blue curve in Fig. 2(b)) with the acquired XPS spectrum (the black curve in Fig. 2(b)), the bond energy t was determined to be -0.2 eV. $q\phi_{S,GaN}$ can be read directly from the lower edge on the theoretical DOS curve (Fig. 2(b)) after obtaining a good fit between the convoluted DOS curve and the measured XPS spectrum around the VBM. For recipe #1-start,
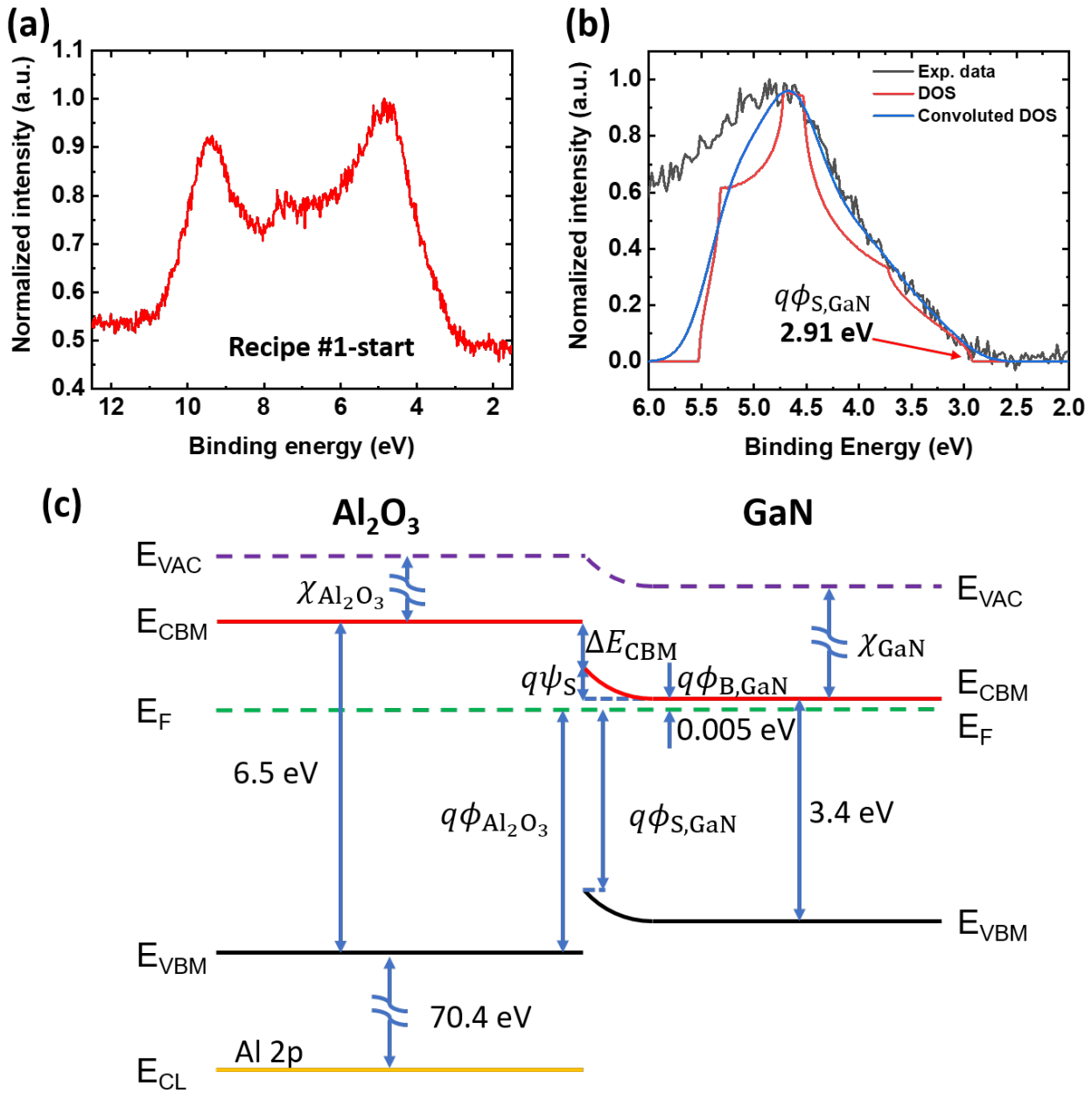
Fig. 2. (a) The valence band XPS spectrum of n-GaN epi (recipe #1-start) directly recorded from the spectrometer. (b) XPS spectrum with a Shirley background subtracted (black line), theoretical DOS curve (red line), and theoretical DOS curve convoluted with the instrumental Gaussian broadening equation (blue line) around the VBM. (c) A Schematic illustration of the band alignment between Al_2O_3 and GaN.

Table 1. Summary of the sample treatment conditions, measured $q\phi_{S,GaN}$, upward band-bending energy values $q\psi_S$, and conduction band barrier height ΔE_{CBM}.

Recipe #	Native oxide removal	ALD cycles (CY)	PDA	$q\phi_{S,GaN}$ (eV)	$q\psi_S$ (eV)	ΔE_{CBM} (eV)
1 (Start)	Yes	-	-	2.91	+0.48	-
2	Yes	5	-	2.96	+0.44	1.57
3	Yes	5	350°C 5 min	3.03	+0.36	1.67
4	Yes	10	-	3.03	+0.37	1.85
5	Yes	10	350°C 5 min	3.09	+0.30	1.75
6	Yes	15	-	3.13	+0.27	1.86
7	Yes	20	-	3.28	+0.12	2.13
1 (End)	Yes	-	-	3.00	+0.39	-

$q\phi_{S,GaN}$ is 2.91 eV (Fig. 2(b)). Combining the GaN bandgap energy ($E_{G,GaN}$) of 3.4 eV and the calculated $q\phi_{B,GaN}$ of 0.005 eV, an upward band-bending ($q\psi_S$) of 0.48 eV was obtained for recipe #1-start from the following equation.

$$q\psi_S = E_{G,GaN} - q\phi_{S,GaN} - q\phi_{B,GaN}, \qquad (2)$$

In this article, we define upward band-bending as positive. Using the identical methods, the $q\phi_{S,GaN}$ and the $q\psi_S$ values of the n-GaN epi under treatment of other recipes were obtained. The $q\psi_S$ values are listed in Table 1 and are also plotted in Fig. 3(a) as a function of the ALD Al₂O₃ deposition cycles.

From the measured XPS spectra, the barrier height ΔE_{CBM} of Al₂O₃ can be calculated using the following relation according to the illustration in Fig. 2(c),

$$\Delta E_{CBM} = \left(E_{G,Al_2O_3} - q\phi_{Al_2O_3}\right) - q\psi_S - (E_{CBM} - E_F)_{GaN}$$

$$= \left(E_{G,Al_2O_3} - [E_{CL} - (E_{CL} - E_{VBM})]_{Al_2O_3}\right) - q\psi_S - q\phi_{B,GaN}, \qquad (3)$$

where ΔE_{CBM} is the conduction band barrier between Al_2O_3 and GaN, E_G is the bandgap, $q\phi_{Al_2O_3}$ is the energy difference between Fermi level and VBM in Al_2O_3, E_{CL} is the binding energy (referred to E_F) of the core level (e.g., Al 2p), and $E_{CL} - E_{VBM}$ is the energy difference between Al 2p core level and the amorphous ALD Al_2O_3 VBM. As mentioned above, E_{CL,Al_2O_3} is selected as Al 2p level, and it has been measured from XPS (Fig. S1). For amorphous ALD Al_2O_3, E_G is adopted as 6.5 eV [21, 29-31], and $E_{CL} - E_{VBM}$ is 70.4 eV [21]. The conduction band barrier height value varies for each recipe and can be calculated, respectively (Table 1). And the band barrier from Al_2O_3 can affect the electrical characteristics of junctions containing interface Al_2O_3, as shown previously [11].

It is worth noting that in the work by Reddy Pramod et al. [25], the bond energy t is chosen to be positive, corresponding to an energy dispersion relation having Γ point as the minimum energy point. Therefore, the energy dispersion relation with a positive t describes the CBM in theory, but not applicable for VBM. While using a positive bond energy t can theoretically lead to incorrect band-bending values, it may not be obvious when a low energy resolution of the instrument (e.g., ~ 0.5 eV in ref. 24) was used, which can smooth out most of the asymmetric features of the theoretical DOS curve after convolution with the Gaussian broadening equation.

As shown in Fig. 3(a), a monotonic trend of the reduction of the upward surface band-bending energy from 0.48 eV down to 0.12 eV was observed as the number of UO Al_2O_3 deposition cycles increased from 0 to 20 cycles. Every additional five-cycle ALD Al_2O_3 deposition resulted in additional band-bending reduction, ranging from 70 meV (from 10 cycles to 5 cycles), 100 meV (from 15 cycles to 10 cycles), and 150 meV (from 20 cycles to 15 cycles). Each PDA procedure caused further band-bending reduction,

ranging from 70 meV (5 cycles annealed) to 60 meV (10 cycles annealed). We expect that the same amount of band-bending reduction may be observed for other cases under the same PDA condition [32].
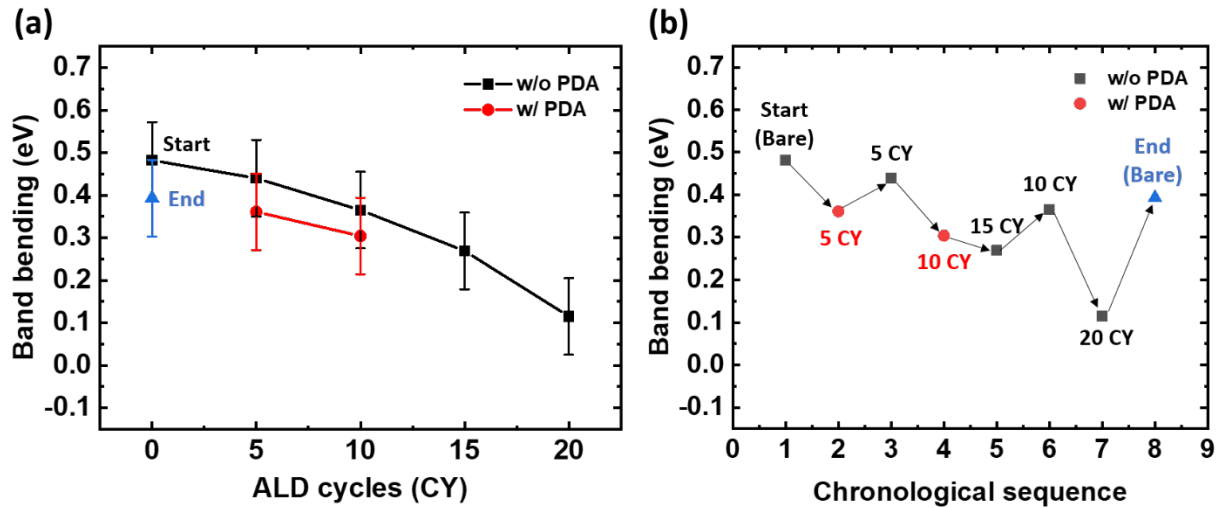

Fig. 3. (a) Plot of the measured surface band-bending values of the n-GaN epi as a function of the number of ALD Al_2O_3 cycles. The lines between the data points are drawn to guide the view of the data. The error bars were estimated based on the standard deviation of Al 2p XPS spectra (0.09 eV). (b) Replot of the data points shown in (a) as a function of the chronological sequence index of the experiment. The arrows between every two data points indicate the experiment sequence.

Since all the surface treatments were performed on the same n-GaN epi sample, to examine how the surface treatments alter the surface conditions of the sample after a series of treatments, the band-bending energy values were replotted as a function of the chronological sequence order, as shown in Fig. 3(b). It is noted that the chronological sequence was not designed intentionally to follow a rough increasing order of the increased number of ALD deposition cycles, instead; it was summarized after all experiments were finished. Fig. 3(b) shows no clear trend of any time-dependence other than the trend that was already shown in Fig. 3(a). Of most importance and interest is the surface band-bending's approximate "recovery" (0.39 eV for the bare/recipe #1-end case) of the n-GaN epi after removing the 20-cycle UO Al_2O_3 layer

that was deposited in recipe #7. The band-bending "recovery" indicates that most of the observed modulation of the upward band-bending (5-20 cycles/recipe #2-#7) was the effect caused by the deposited UO Al_2O_3. The remaining difference (0.09 eV) between recipe #1-start and recipe #1-end could be due to the uncertainty of the experiments or, to a small speculated extent, due to the removal/oxidation of some Ga atoms from the epi surface and thus the associated change of the density of polarization charges at the surface caused by the series of surface treatments. Nevertheless, Fig. 3 clearly indicates that UO Al_2O_3 deposition on GaN surface can reduce the upward band-bending of Ga-face, c-plane GaN, and more cycles of Al_2O_3 deposition can have more effect on the reduction of the upward band-bending.

There are multiple theories about charge compensation by ALD Al_2O_3 on III-nitride surface. The community has reported in metal-oxide-semiconductor (MOS) GaN structure that the interface fixed charge between Al_2O_3 and III-nitride can be changed from intrinsic negative charge to positive charge [18-20, 32, 33] and proposed multiple hypotheses of the mechanisms. We analyzed these reported theories to identify the most plausible one that is applicable to our results. Theory #1: Esposto et al. proposed the charge compensation theory based on the polarization inversion due to the Ga-O bonds formation [18]. However, Ga-O bonds exist on the measured surfaces from recipe #2 to #7 (see Fig. S4) and thus they are unlikely to be the reason for the change of surface fixed charges in this work. Furthermore, polarization inversion was not observed in this study. Theory #2: Ganguly et al. and Ťapajna et al. treated oxygen atoms as donor dopants in GaN, which contribute positive fixed charges at the surface of GaN [32, 33]. But for recipes #2 to #7, all surfaces have more than the sufficient number of oxygen atoms to substitute the nitrogen sites on the surface [33], meaning that the same band-bending should be measured through these recipes if the theory holds true, which is also contrary to the results observed in this work. Theory #3: Ťapajna et al. and Hayashi et al. developed the hypothesis that donor-type surface defects act as positive fixed surface charges on GaN [19, 34]. However, the trap state density on the surface with ALD Al_2O_3 has been experimentally found to decrease with the increasing number of ALD cycles previously

[35, 36]. Therefore, one would expect to see a weaker compensation effect with more cycles of ALD Al_2O_3. This is opposite to what we have observed in our work. Theory #4: Bakeroot et al. proposed the border trap theory [37]. According to this theory, if we assume a uniform density of traps inside the insulator (Al_2O_3) along the deposition direction, about 5 nm of Al_2O_3 would be needed to achieve the polarization inversion that has been observed in a GaN MOS structure, based on the trend observed in this work. As a matter of fact, it is questionable whether the insulator traps located at this distance away from the interface can still have influence on GaN. Theory #5: Esposto et al. and Matys et al. proposed that the charge compensation mechanism at the energy states between the CBMs of the UO and that of GaN [18, 38] can cause the change of band-bending. The band structure and the density of states in the band gap of UO Al_2O_3 can possibly change with different numbers of cycles therefore, providing different degrees of charge compensation effects. It is therefore believed that the charge compensation mechanism as described in the theory by Esposto et al. [18] and Matys et al. [38] is the most probable one that is responsible for the observed band-bending in this work.

The demonstrated modulation/suppression of energy band-bending at the n-GaN surface enabled by the UO Al_2O_3 implies the potential to develop practical AlGaAs/GaAs/GaN HBTs employing the grafting approach [11]. To illustrate this implication, an AlGaAs/GaAs/GaN npn HBT with a vertical layer structure shown in Fig. S5(a) and Fig. S6(a) was simulated using Silvaco® device simulator Atlas® (Fig. S5(b) and Fig. S6(b)). The emitter and base layers of the HBT used in the simulations are identical to those of the AlGaAs/GaAs/GaN HBT fabricated using wafer fusion [8]. The only major difference between the fused HBT [8] and the simulated HBT is the UO Al_2O_3 interface between the p+ GaAs (base) and the n- GaN (collector) in the latter case. To perform the HBT simulations, the UO Al_2O_3 at the interface was treated in two ways. In Case 1 (Fig. S5), it is considered an ideal interface (i.e., ignoring the existence of the Al_2O_3) given the ideal p-n junction that can be achieved in grafting ($n \sim 1.09$ or less) [11]. In Case 2 (Fig. S6), the UO Al_2O_3 is considered an insulator. The detailed settings and descriptions of the

simulations can be found in the Supplementary Information (SI). It is noted that the UO Al_2O_3 functions as a double-sided passivation and quantum tunneling layer. Therefore, neither of the two treatment methods accurately captures the physical charge carrier transport mechanisms in a real grafted GaAs/GaN pn junction at this stage of the simulations study.

Fig. S5(d) shows the simulated current gain (β) values of the HBT as a function of the base-emitter voltage (V_{BE}) at collector-emitter voltage (V_{CE}) of 5 V, under different surface treatment conditions, for Case 1. The observed increasing trend of the β values as the surface band-bending energy of GaN, the only variable in the simulations, decreases reflects the direct correlation between GaN surface band-bending and the HBT transistor action. Since the effects of the UO Al_2O_3 layer were not taken into account in the simulations, the β values obtained from the simulations are considered an overestimate.

Fig. S6(d) shows the simulated β values of the HBT as a function of V_{BE} under collector-base voltage V_{CB} of 3 V for Case 2. It is noted that because the UO Al_2O_3 is considered as an insulator in this case, the polarization of the GaN cannot implemented in the simulator. The β at higher V_{CB} cannot be simulated due to convergence problems encountered in the simulations, which is further due to the insulator setting for the Al_2O_3 layer. In this case, only recipe #3 can lead to a useful β value (30). Given that the UO Al_2O_3 layer is a conductor layer, treating the layer as an insulator has underestimated the β values of the HBT on one hand. On the other hand, the setting of no polarization should have overestimated the β value. While a more accurate modeling approach that can better depict the physical behavior of the Al_2O_3 layer in the grafted system needs to be developed, the simulations under the two extreme conditions (Case I and Case II) together with the band-bending characterizations in this work have allowed one to peek into the potential of implementing AlGaAs/GaAs/GaN npn HBTs using the grafting approach.

It is noted that although AlGaAs/GaAs/GaN npn HBT was envisioned and used as the GaN-collector HBT example in the simulation study, the principle of the GaN-collector HBT work mechanism is also

applicable to several other suitable material combinations (e.g., npn Si/Ge/GaN, npn GaAs/Si/GaN, npn GaAs/Ge/GaN etc., to name a few) provided that the conduction band alignment of the constituent materials is appropriated for electron transport in the bipolar transistor action mode and that, from a practical point of view, the material combinations are implementable via the grafting approach [11]. Future device fabrication work using the grafting approach will be needed to experimentally verify the GaN-collector HBT prospective, along with characterization of the interface such as interface trap distribution in the bandgap [39] to help us better understand the grafted interface with UO.

Conclusion

In summary, it is shown that the essential UO Al_2O_3 needed at the GaAs/GaN interface in grafting can help suppress the upward band-bending of c-plane, Ga-face GaN with a monotonic trend of suppression enhancement following the increase of the Al_2O_3 thickness. Employing 20 cycles ALD Al_2O_3 can suppress the band-bending of GaN from 0.48 eV of a bare GaN down to 0.12 eV. Preliminary device simulations show that the suppression of upward band-bending with proper UO thickness can potentially improve the current gain of AlGaAs/GaAs/GaN npn HBT with a grafted base-collector junction, implying the prospective of development of practical GaN-collector HBTs. New experimental work is in progress to further examine the electrical effects from both the band barrier of Al_2O_3 and the observed band-bending of GaN.

Acknowledgement

References:

[1] M. W. Moseley, A. A. Allerman, M. H. Crawford, J. J. Wierer Jr, M. L. Smith, and A. M. Armstrong, "Detection and modeling of leakage current in AlGaN-based deep ultraviolet light-emitting diodes," *Journal of Applied Physics,* vol. 117, no. 9, p. 095301, 2015.

[2] P. Siddiqua, W. A. Hadi, M. S. Shur, and S. K. O'Leary, "A 2015 perspective on the nature of the steady-state and transient electron transport within the wurtzite phases of gallium nitride, aluminum nitride, indium nitride, and zinc oxide: a critical and retrospective review," *Journal of Materials Science: Materials in Electronics,* vol. 26, no. 7, pp. 4475-4512, 2015.

[3] Y. Tang *et al.*, "Ultrahigh-speed GaN high-electron-mobility transistors with f_{T}/f_{max} of 454/444 GHz," *IEEE Electron Device Letters,* vol. 36, no. 6, pp. 549-551, 2015.

[4] M. Asif Khan, J. Kuznia, D. Olson, W. Schaff, J. Burm, and M. Shur, "Microwave performance of a 0.25 µm gate AlGaN/GaN heterostructure field effect transistor," *Applied Physics Letters,* vol. 65, no. 9, pp. 1121-1123, 1994.

[5] S. M. Sze, Y. Li, and K. K. Ng, *Physics of semiconductor devices*. John wiley & sons, 2021.

[6] L. S. McCarthy *et al.*, "GaN HBT: toward an RF device," *IEEE Transactions on Electron Devices,* vol. 48, no. 3, pp. 543-551, 2001.

[7] C. Lian, H. Xing, C. S. Wang, L. McCarthy, and D. Brown, "DC characteristics of AlGaAs/GaAs/GaN HBTs formed by direct wafer fusion," *IEEE electron device letters,* vol. 28, no. 1, pp. 8-10, 2006.

[8] C. Lian, H. G. Xing, C. S. Wang, D. Brown, and L. McCarthy, "Gain degradation mechanisms in wafer fused Al Ga As ∕ Ga As ∕ Ga N heterojunction bipolar transistors," *Applied Physics Letters,* vol. 91, no. 6, p. 063502, 2007.

[9] D. Zubia, S. H. Zaidi, S. Brueck, and S. Hersee, "Nanoheteroepitaxial growth of GaN on Si by organometallic vapor phase epitaxy," *Applied Physics Letters,* vol. 76, no. 7, pp. 858-860, 2000.

[10] T. Araki *et al.*, "Radio-frequency plasma-excited molecular beam epitaxy growth of GaN on graphene/Si (100) substrates," *Applied Physics Express,* vol. 7, no. 7, p. 071001, 2014.

[11] D. Liu *et al.*, "Lattice-mismatched semiconductor heterostructures," *arXiv preprint arXiv:1812.10225,* 2018/12/26 2018.

[12] D. Liu *et al.*, "229 nm UV LEDs on aluminum nitride single crystal substrates using p-type silicon for increased hole injection," *Applied Physics Letters,* vol. 112, no. 8, p. 081101, 2018.

[13] D. Liu *et al.*, "226 nm AlGaN/AlN UV LEDs using p-type Si for hole injection and UV reflection," *Applied Physics Letters,* vol. 113, no. 1, p. 011111, 2018.

[14] S. J. Cho *et al.*, "P-type silicon as hole supplier for nitride-based UVC LEDs," *New Journal of Physics,* vol. 21, no. 2, p. 023011, 2019.

[15] S. J. Cho *et al.*, "Fabrication of AlGaAs/GaAs/diamond heterojunctions for diamond-collector HBTs," *AIP Advances,* vol. 10, no. 12, p. 125226, 2020.

[16] M. E. Levinshtein, S. L. Rumyantsev, and M. S. Shur, *Properties of Advanced Semiconductor Materials: GaN, AIN, InN, BN, SiC, SiGe*. John Wiley & Sons, 2001.

[17] T. Chow and M. Ghezzo, "SiC power devices," *MRS Online Proceedings Library (OPL),* vol. 423, 1996.

[18] M. Esposto, S. Krishnamoorthy, D. N. Nath, S. Bajaj, T.-H. Hung, and S. Rajan, "Electrical properties of atomic layer deposited aluminum oxide on gallium nitride," *Applied Physics Letters,* vol. 99, no. 13, p. 133503, 2011.

[19] M. Ťapajna and J. Kuzmík, "A comprehensive analytical model for threshold voltage calculation in GaN based metal-oxide-semiconductor high-electron-mobility transistors," *Applied Physics Letters,* vol. 100, no. 11, p. 113509, 2012.

[20] J. Son, V. Chobpattana, B. M. McSkimming, and S. Stemmer, "Fixed charge in high-k/GaN metal-oxide-semiconductor capacitor structures," *Applied Physics Letters,* vol. 101, no. 10, p. 102905, 2012.

[21]   J. Yang, B. S. Eller, C. Zhu, C. England, and R. J. Nemanich, "Comparative band alignment of plasma-enhanced atomic layer deposited high-k dielectrics on gallium nitride," *Journal of Applied Physics,* vol. 112, no. 5, p. 053710, 2012.

[22]   E. Ber, B. Osman, and D. Ritter, "Measurement of the variable surface charge concentration in gallium nitride and implications on device modeling and physics," *IEEE Transactions on Electron Devices,* vol. 66, no. 5, pp. 2100-2105, 2019.

[23]   R. L. Puurunen, "Analysis of hydroxyl group controlled atomic layer deposition of hafnium dioxide from hafnium tetrachloride and water," *Journal of applied physics,* vol. 95, no. 9, pp. 4777-4786, 2004.

[24]   Q. Paduano, M. Snure, G. Siegel, D. Thomson, and D. Look, "Growth and characteristics of AlGaN/GaN heterostructures on sp2-bonded BN by metal–organic chemical vapor deposition," *Journal of Materials Research,* vol. 31, no. 15, pp. 2204-2213, 2016.

[25]   P. Reddy *et al.*, "The effect of polarity and surface states on the Fermi level at III-nitride surfaces," *Journal of Applied Physics,* vol. 116, no. 12, p. 123701, 2014.

[26]   P. Citrin, G. Wertheim, and Y. Baer, "Surface-atom x-ray photoemission from clean metals: Cu, Ag, and Au," *Physical Review B,* vol. 27, no. 6, p. 3160, 1983.

[27]   S. Peters, S. Peredkov, M. Neeb, W. Eberhardt, and M. Al-Hada, "Size-dependent XPS spectra of small supported Au-clusters," *Surface science,* vol. 608, pp. 129-134, 2013.

[28]   P. Reddy *et al.*, "Charge neutrality levels, barrier heights, and band offsets at polar AlGaN," *Applied Physics Letters,* vol. 107, no. 9, p. 091603, 2015.

[29]   H. Yu *et al.*, "Energy gap and band alignment for (HfO 2) x (Al 2 O 3) 1− x on (100) Si," *Applied Physics Letters,* vol. 81, no. 2, pp. 376-378, 2002.

[30]   H. Yu, M. Li, and D. Kwong, "ALD (HfO2) x (Al2O3) 1− x high-k gate dielectrics for advanced MOS devices application," *Thin Solid Films,* vol. 462, pp. 110-113, 2004.

[31] N. V. Nguyen *et al.*, "Band offsets of atomic-layer-deposited Al 2 O 3 on GaAs and the effects of surface treatment," *Applied Physics Letters,* vol. 93, no. 8, p. 082105, 2008.

[32] M. Ťapajna *et al.*, "Investigation of 'surface donors' in Al2O3/AlGaN/GaN metal-oxide-semiconductor heterostructures: Correlation of electrical, structural, and chemical properties," *Applied Surface Science,* vol. 426, pp. 656-661, 2017.

[33] S. Ganguly, J. Verma, G. Li, T. Zimmermann, H. Xing, and D. Jena, "Presence and origin of interface charges at atomic-layer deposited Al2O3/III-nitride heterojunctions," *Applied physics letters,* vol. 99, no. 19, p. 193504, 2011.

[34] Y. Hayashi, S. Sugiura, S. Kishimoto, and T. Mizutani, "AlGaN/GaN MOSHFETs with HfO2 gate oxide: A simulation study," *Solid-state electronics,* vol. 54, no. 11, pp. 1367-1371, 2010.

[35] J. Schmidt, B. Veith, and R. Brendel, "Effective surface passivation of crystalline silicon using ultrathin Al2O3 films and Al2O3/SiNx stacks," *physica status solidi (RRL)–Rapid Research Letters,* vol. 3, no. 9, pp. 287-289, 2009.

[36] F. Werner *et al.*, "Electronic and chemical properties of the c-Si/Al2O3 interface," *Journal of Applied Physics,* vol. 109, no. 11, p. 113701, 2011.

[37] B. Bakeroot *et al.*, "On the origin of the two-dimensional electron gas at AlGaN/GaN heterojunctions and its influence on recessed-gate metal-insulator-semiconductor high electron mobility transistors," *Journal of Applied Physics,* vol. 116, no. 13, p. 134506, 2014.

[38] M. Matys, R. Stoklas, M. Blaho, and B. Adamowicz, "Origin of positive fixed charge at insulator/AlGaN interfaces and its control by AlGaN composition," *Applied physics letters,* vol. 110, no. 24, p. 243505, 2017.

[39] J. K. Kaushik, V. Balakrishnan, B. Panwar, and R. Muralidharan, "Inverse temperature dependence of reverse gate leakage current in AlGaN/GaN HEMT," *Semiconductor science and technology,* vol. 28, no. 1, p. 015026, 2012.

Supplementary Information:

Influences of ALD Al₂O₃ on the surface band-bending of c-plane, Ga-face GaN and the implication to GaN-collector npn heterojunction bipolar transistors

Jiarui Gong[1], Jisoo Kim[2], TienKhee Ng[3], Kuangye Lu[4], Donghyeok Kim[2], Jie Zhou[2], Dong Liu[2], Jeehwan Kim[4], Boon S. Ooi[3], and Zhenqiang Ma[2,a]

[1]*Department of Physics, University of Wisconsin-Madison, Madison, Wisconsin, 53706,*

USA

[2]*Department of Electrical and Computer Engineering, University of Wisconsin-Madison,*

Madison, Wisconsin, 53706, USA

[3]*Department of Electrical and Computer Engineering, King Abdullah University of*

Science and Technology, Thuwal 23955-6900, Saudi Arabia

[4]*Department of Mechanical Engineering, Department of Materials Science and*

Engineering, Massachusetts Institute of Technology, Cambridge, Massachusetts, 02139,

USA

[a]   Author to whom correspondence should be addressed. Electronic mail: mazq@engr.wisc.edu

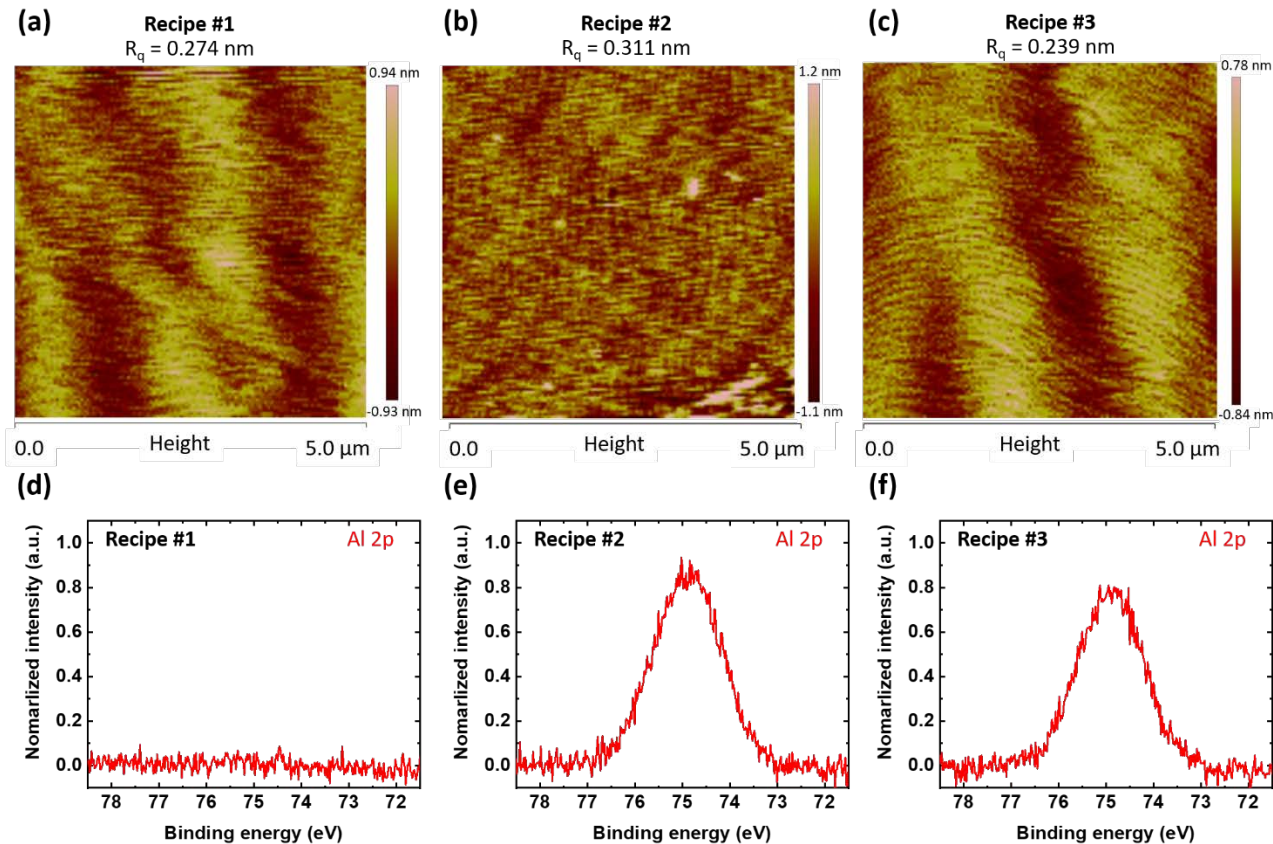# I. Atomic Force Spectroscopy (AFM) images of the n-GaN Epitaxial Samples

Fig. S1. AFM images and Al 2p XPS spectra of the n-GaN epi sample under different surface treatment conditions: (a) $R_q = 0.274$ nm and (d) for recipe #1: bare surface, (b) $R_q = 0.311$ nm and (e) for recipe #2: 5-cycle ALD Al_2O_3 coating, and (c) $R_q = 0.239$ nm and (f) for recipe #3: 5-cycle ALD Al_2O_3 coating and PDA.

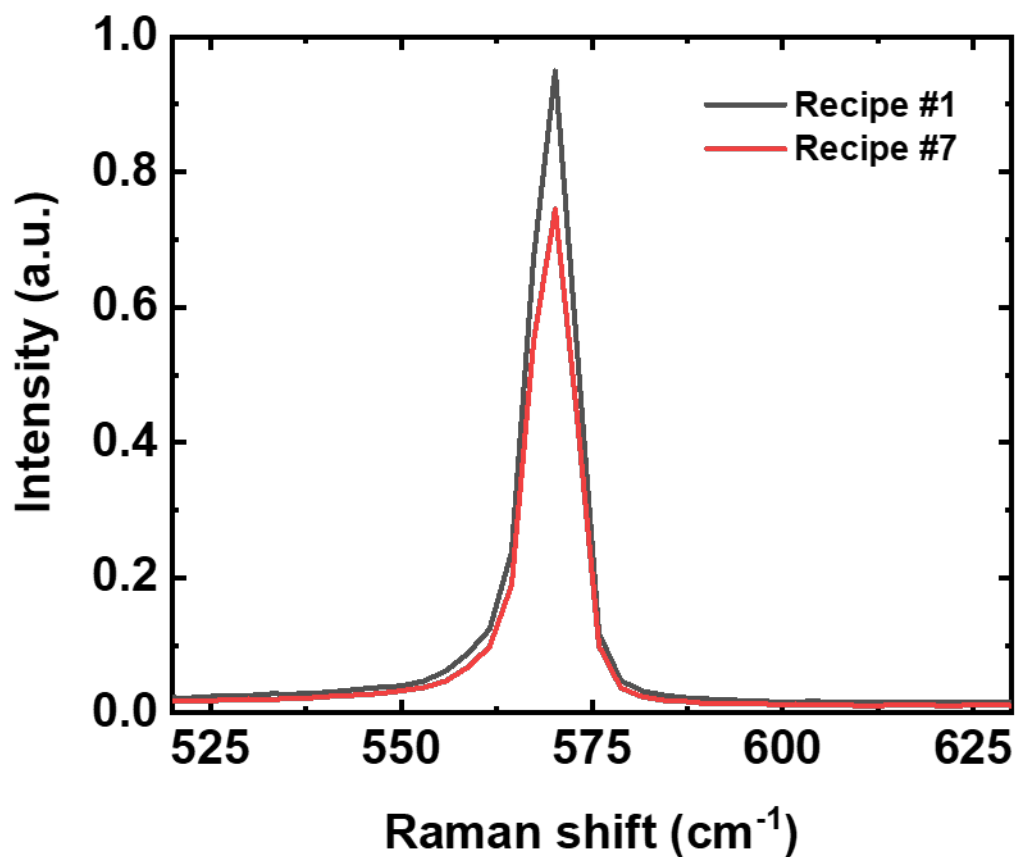**II.   Raman Spectroscopy Analysis of the n-GaN Epitaxial Samples**

Fig. S2. Raman spectra of recipe #1 (bare) and recipe #7 (20 cycles).

We performed Raman spectroscopy analysis to assess the stress status of the n-GaN epitaxial layer. Raman spectra were performed using a Raman microscopic system (α 300M+, WITec) with a pump laser wavelength of 532 nm and an objective lens of 100× magnification. As shown in Fig. S2, we measured the frequency shift of the E_2 high (E_2^H) mode of GaN, which is a good representation of biaxial strain in c-plane GaN [1]. For relaxed GaN, the E_2^H mode phonon frequency is observed at 568 cm^{-1} [2]. For our n-GaN epi on sapphire, it is measured at 570 cm^{-1} for both recipes #1 and #7, which matches the reported value for GaN on sapphire [1] and exhibits compressive stress. The results show that the ALD Al_2O_3 does not introduce additional stress to the GaN epi.

III. XPS Spectra and fitting of the n-GaN Epitaxial Samples

(a) Recipe #2

(b) Recipe #3

(c) Recipe #4

(d) Recipe #5

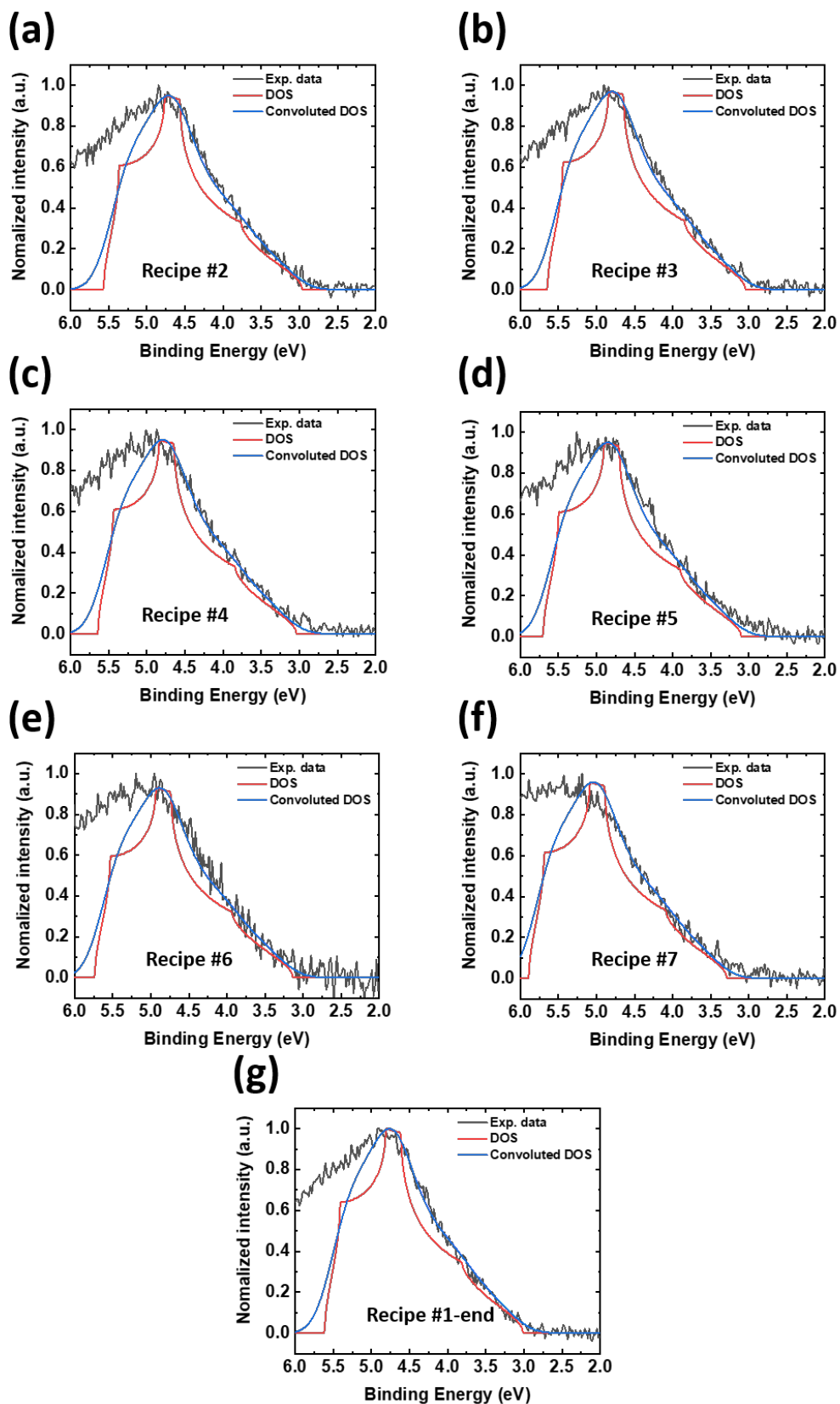(e) Recipe #6

(f) Recipe #7

(g) Recipe #1-end

Fig. S3. XPS spectra with a Shirley background subtracted (black line), theoretical DOS curve (red line), and theoretical DOS curve convoluted with the instrumental Gaussian broadening equation (blue line) around the VBM for recipes #2 (a) to #7 (f) and recipe #1-end (g).

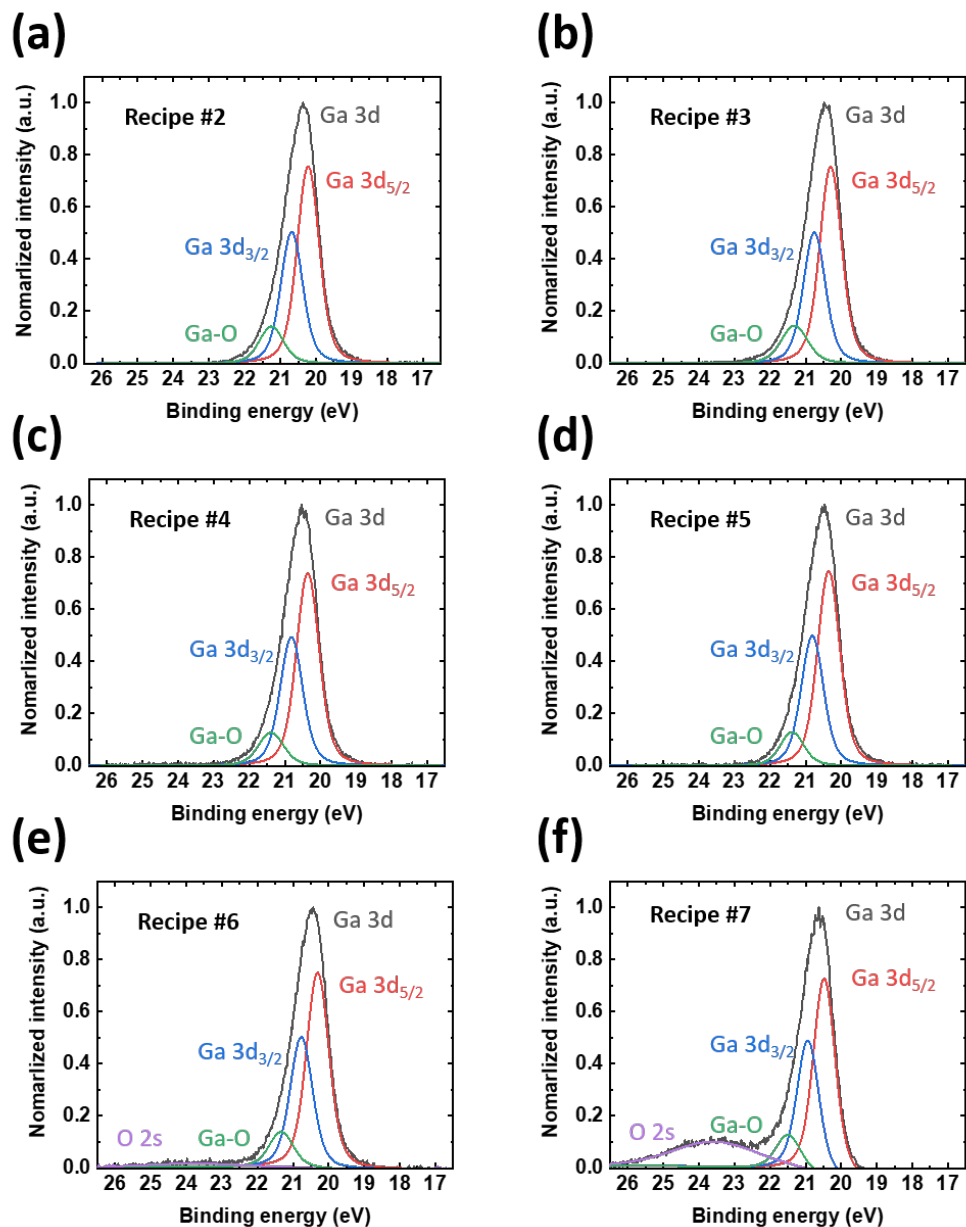## IV.   Ga 3d XPS Spectra of the n-GaN Epitaxial Samples

Fig. S4. Ga 3d XPS spectra of recipes #2 (a) to #7(f). A Sherley background is subtracted from each spectrum.

V.   AlGaAs/GaAs/GaN npn HBT Simulations

The present device simulators are unable to accurately model the charge carrier transport across the ultrathin dielectric layer (Al_2O_3) used in grafted semiconductor material systems because the interface Al_2O_3 layer is treated as an insulator, while the roles of the Al_2O_3 layer are double-side passivation and quantum tunneling glue layer allowing both electrons and holes to tunnel through [3]. As a result, the Al_2O_3 layer behaves like a super-wideband semiconductor, forming double interfaces with its neighboring semiconductors with finite (very low) densities of states. Based on these considerations, we provide simulation results of the AlGaAs/GaAs/GaN npn HBT under two extreme conditions using Silvaco® device simulator Atlas®: 1) treating the GaAs/GaN interface as an ideal interface (i.e., ignoring the existence of the Al_2O_3 layer), under which condition the HBT performance should be overestimated; and 2) treating the Al_2O_3 layer as an insulator, under which condition the HBT performance should be underestimated due to the poorer conductivity of the insulator than the reality, where the Al_2O_3 layer is an effective electron/hole conductor. We expect that an accurately predicted HBT performance, upon the development and availability of a suitable model for modeling the grafted material system, would lie in between the results of these two extreme conditions.

Case I: Treating the GaAs/GaN interface as an ideal interface

Since the grafted interface between GaAs and GaN can have an ideal p-n junction ($n \sim 1.09$ or less) [3], the GaAs/GaN junction was treated as an epitaxy-like junction in the simulations in this case. Under this ideal assumption, the only material variable parameter in the simulations is the polarization scaler of the GaN, which was set according to the measured corresponding band-bending values listed in Table 1 (also shown in Fig. 3).
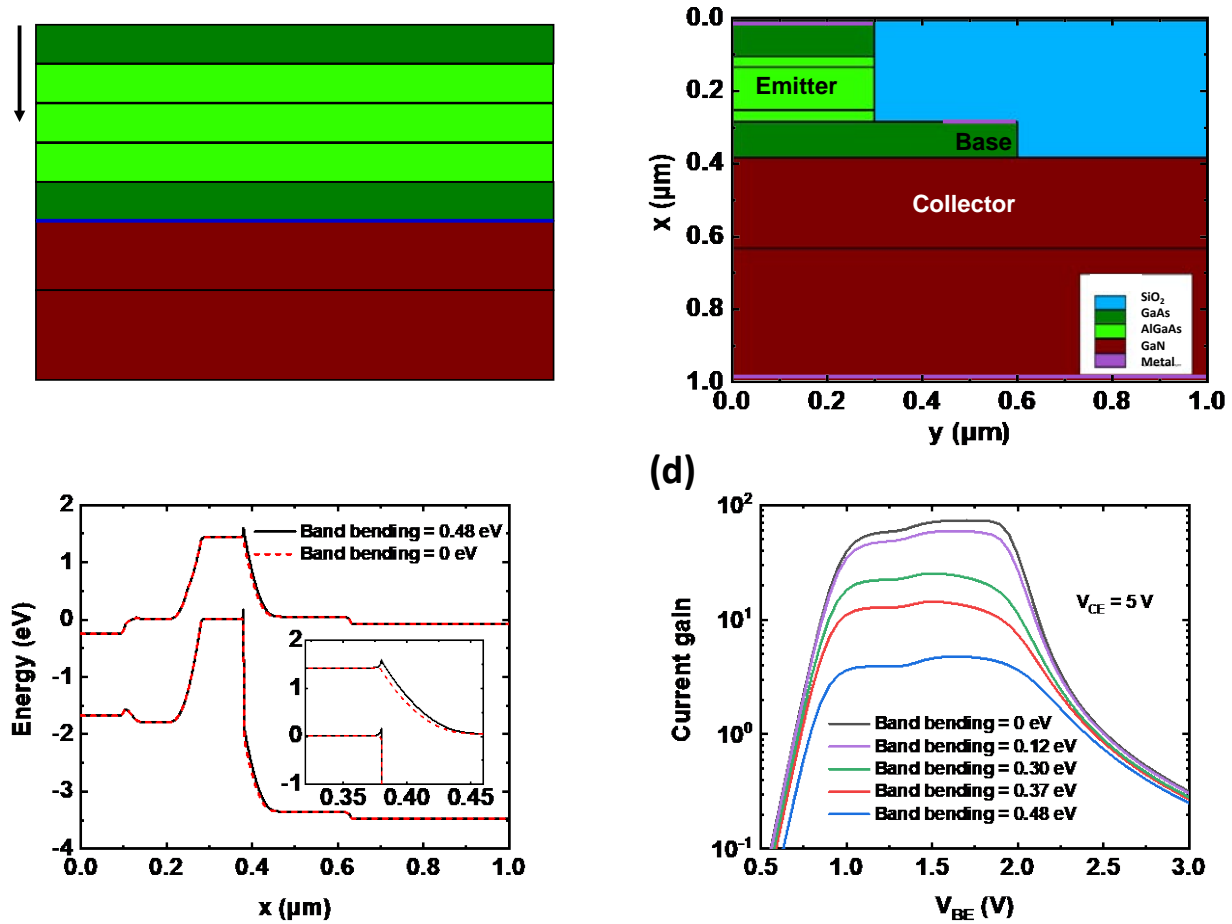
Fig. S5. Case I. (a) Schematic layer structure of an AlGaAs/GaAs/GaN npn HBT with ALD Al$_2$O$_3$ at the interface of GaAs/GaN. (b) Simulated AlGaAs/GaAs/GaN npn HBT structure at the interface of Silvaco$^®$. (c) Simulated band diagram at zero bias of the AlGaAs/GaAs/GaN npn HBT with 0.48 eV band-bending (black solid lines) and 0 eV band-bending (red dashed lines). The inset is the enlarged region around the GaAs/GaN heterojunction showing the detailed band structure at the GaAs/GaN interface. (d) Simulated current gain β versus base-emitter voltage V_{BE} at V_{CE} of 5 V under different n-GaN upward band-bending values. In the simulations, only the band-bending energy value varied.

Fig. S5(a) shows a schematic illustration of the simulated HBT structure (the Al$_2$O$_3$ layer was only treated as an ideal double-side passivation layer and not inserted physically in the simulation). The emitter and base layers of the HBT (Fig. S5(a)) used in the simulations are identical to that of the

AlGaAs/GaAs/GaN HBT fabricated using wafer fusion [4]. Fig. S5(b) shows the HBT structure in Atlas®

interface. Fig. S5(c) shows the simulated band diagrams of the HBT with the n-GaN as the HBT collector

having an upward band-bending of 0.48 eV (recipe #1-start) and having zero upward band-bending (an

imagined extreme situation) for comparison. The inset of Fig. S5(c) shows an enlarged view of the

comparison of the band alignment at the base-collector junction under the two band-bending situations.

The simulated current gain (β) values of the HBT as a function of the base-emitter voltage (V_{BE}) at

collector-emitter voltage (V_{CE}) of 5 V, under different upward band-bending energies, are plotted in Fig.

S5(d). From Fig. S5(d), one can see that the GaN polarization-induced upward band-bending substantially

reduces the HBT current gain from 74 (0 eV band-bending) to 4.8 for the bare GaN (0.48 eV band-

bending). The results indicate that with an ideally passivated interface between GaAs and c-plane, Ga-

face GaN, like what was already experimentally achieved [3], developing practical GaN-collector HBT is

nearly impossible due to the electron transport barrier created by upward band-bending of the c-plane, Ga-

face GaN. Nevertheless, the UO Al_2O_3 at the interface of GaAs and GaN with proper thicknesses could

lead to both an ideal pn junction and a suitable band alignment at the p-GaAs/n-GaN base-collector

junction, facilitating electron transport from the AlGaAs emitter, crossing the GaAs base, and collected

by the GaN collector. Specifically, with a 20-cycle ALD Al_2O_3 layer (i.e., 0.12 eV upward band-bending

as measured from the XPS in this study), the β can reach 59, slightly lower than the ideal case (no band-

bending) but 12 times higher than that of bare GaN. Although the effects of the UO Al_2O_3 on the electrical

characteristic of the HBT have not been considered, the simulations together with the band-bending

characterizations in this work have shed light on the promising route toward GaN-collector HBTs.

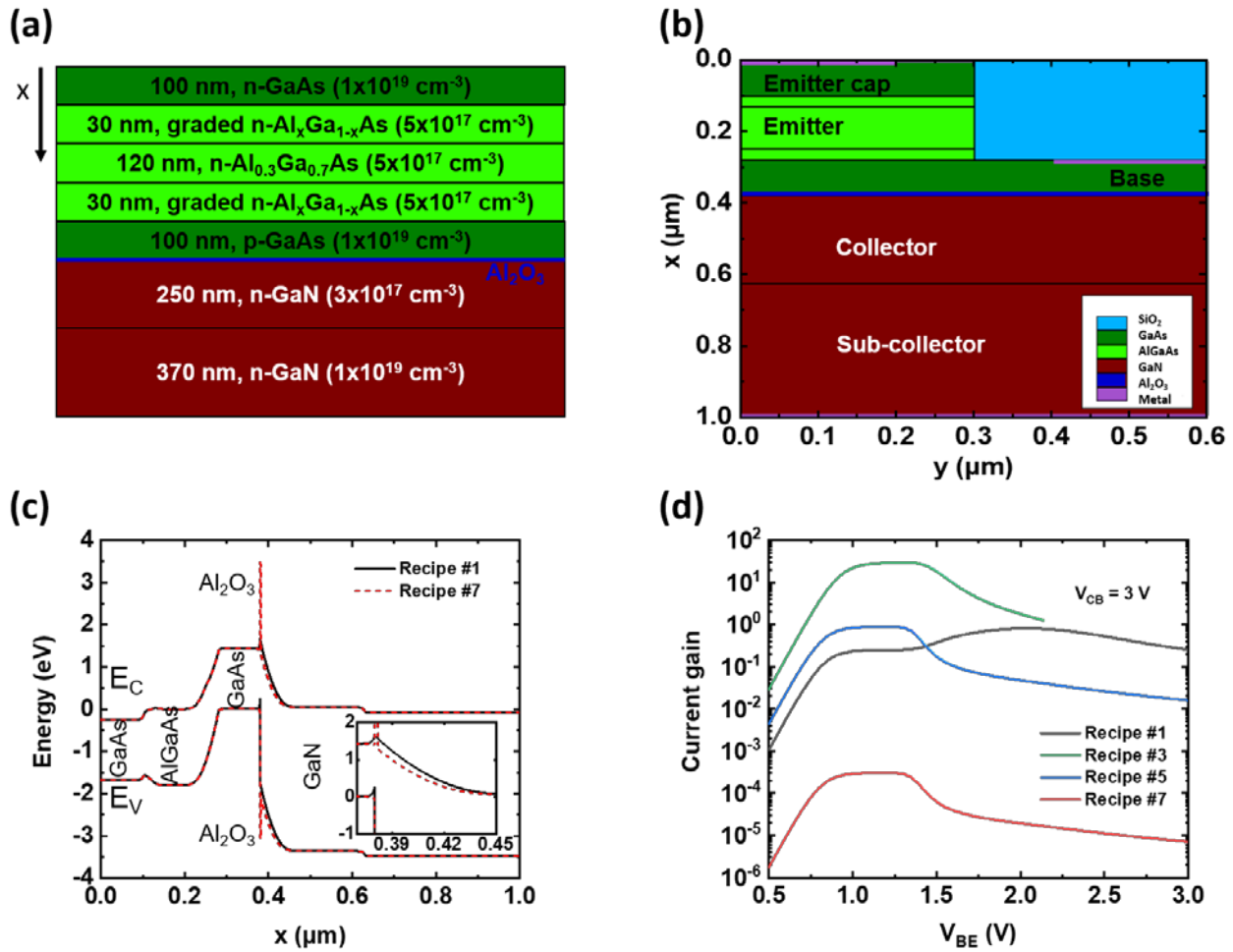*Case II. Treating the Al_2O_3 layer as an insulator*

Fig. S6. Case II. (a) Schematic layer structure of an AlGaAs/GaAs/GaN npn HBT with ALD Al₂O₃ (as insulator) at the interface of GaAs/GaN. (b) Simulated device structure at the interface of Silvaco®. (c) Simulated band diagram at zero bias of the AlGaAs/GaAs/GaN npn HBT of surface treatment recipe #1 (black solid lines) and recipe #7 (red dashed lines). The inset is the enlarged region around the GaAs/GaN heterojunction showing the detailed band structure at the GaAs/GaN interface. (d) Simulated current gain β versus base-emitter voltage V_{BE} at V_{CB} of 3 V under different surface treatments.

In this case, the identical layer structure to Fig. S5(a) was used, except that the Al₂O₃ interlayer was inserted as an insulator layer and the tunneling models (sis.el and sis.ho) were applied to the base/collector junction in the simulation (Fig. S5(b)).

Fig. S6(c) shows the simulated band diagram of the HBT with n-GaN as the HBT collector having an upward band-bending of 0.48 eV (recipe #1-start) and 0.12 eV (i.e., the 20-cycle Al_2O_3 coated GaN collector: recipe #7)) for comparison. The inset of Fig. S6(c) shows an enlarged view of the comparison of the band alignment at the base-collector junction. The simulated β values of the HBT as a function of V_{BE} at collector-base voltage (V_{CB}) of 3 V, under different surface treatment conditions, are plotted in Fig. S6(d). From Fig. S6(d), one can see that a balance between effective quantum tunneling across the "insulator" layer and sufficient suppression of upward band-bending is achieved for recipe #3. The GaN polarization-induced upward band-bending substantially reduces the HBT current gain from 30 (recipe #3) to 0.8 for the bare GaN (recipe #1). Due to the strong insulating effects of the Al_2O_3 layer, the current gain was less than 1 for recipes #5 and #7. Since the Al_2O_3 layer is not an insulator in our material system, it is highly likely that the simulation in this case has underestimated the performance of the HBT.

Considering that neither of the two simulations can provide accurate predictions of the HBT performance, the simulation results can be regarded as a rough performance range estimation (from the best scenario, Case I, to the worst, Case II) of the HBT. While an accurate modeling approach is needed to simulate the grafted material systems, device fabrication work using the grafting approach will be needed to experimentally verify the GaN-collector HBT prospective, along with characterization of the interface such as interface trap distribution in the bandgap [5] to help us better understand the grafted interface with UO.

References

[1]   Q. Paduano, M. Snure, G. Siegel, D. Thomson, and D. Look, "Growth and characteristics of AlGaN/GaN heterostructures on sp2-bonded BN by metal–organic chemical vapor deposition," *Journal of Materials Research,* vol. 31, no. 15, pp. 2204-2213, 2016.

[2]   H. Harima, "Properties of GaN and related compounds studied by means of Raman scattering," *Journal of Physics: Condensed Matter,* vol. 14, no. 38, p. R967, 2002.

[3]   D. Liu *et al.*, "Lattice-mismatched semiconductor heterostructures," *arXiv preprint arXiv:1812.10225,* 2018/12/26 2018.

[4]   C. Lian, H. G. Xing, C. S. Wang, D. Brown, and L. McCarthy, "Gain degradation mechanisms in wafer fused $Al\,Ga\,As\,/\,Ga\,As\,/\,Ga\,N$ heterojunction bipolar transistors," *Applied Physics Letters,* vol. 91, no. 6, p. 063502, 2007.

[5]   J. K. Kaushik, V. Balakrishnan, B. Panwar, and R. Muralidharan, "Inverse temperature dependence of reverse gate leakage current in AlGaN/GaN HEMT," *Semiconductor science and technology,* vol. 28, no. 1, p. 015026, 2012.